Development 140, 4041-4050 (2013) doi:10.1242/dev.096255

Dynamic responses of endothelial cells to changes in blood flow during vascular remodeling of the mouse yolk sac

Ryan S. Udan, Tegy J. Vadakkan and Mary E. Dickinson*

SUMMARY

Despite extensive work showing the importance of blood flow in angiogenesis and vessel remodeling, very little is known about how changes in vessel diameter are orchestrated at the cellular level in response to mechanical forces. To define the cellular changes necessary for remodeling, we performed live confocal imaging of cultured mouse embryos during vessel remodeling. Our data revealed that vessel diameter increase occurs via two distinct processes that are dependent on normal blood flow: vessel fusions and directed endothelial cell migrations. Vessel fusions resulted in a rapid change in vessel diameter and were restricted to regions that experience the highest flow near the vitelline artery and vein. Directed cell migrations induced by blood flow resulted in the recruitment of endothelial cells to larger vessels from smaller capillaries and were observed in larger artery segments as they expanded. The dynamic and specific endothelial cell behaviors captured in this study reveal how sensitive endothelial cells are to changes in blood flow and how such responses drive vascular remodeling.

KEY WORDS: Cell migration, Endothelial cell, Mouse, Vascular remodeling, Vessel fusion, Yolk sac

INTRODUCTION

During mammalian development, the embryo is initially supported by simple diffusion of the necessary gases and molecules, but undergoes a critical physiological transition in which the embryo becomes dependent on blood circulation to support further development. In the mouse embryo, this transition occurs shortly after the circulatory system becomes functional on embryonic day (E) 8.0 (3-somite stage) when the heart begins to beat (Lucitti et al., 2007; Udan et al., 2013). Shortly thereafter, primitive erythroblasts enter the circulation and the vasculature remodels to facilitate the distribution of blood and provide efficient transport through the embryo and to extra-embryonic regions such as the yolk sac. Remodeling of the yolk sac vasculature becomes evident as the initial primitive plexus, consisting of small diameter capillaries (mostly within 30-70 μm), is transformed from E8.5 to E9.5 into a branched tree-like structure with a hierarchical arrangement of large diameter vessels (150-230 μm) leading to progressively smaller diameter vessels on both the venous and arterial sides (Fig. 1A-D).

Vessel remodeling is crucial to embryo survival at this early stage. A survey of the literature reveals that over 100 different single gene mutations have been identified that disrupt remodeling from E8.5 to E9.5 resulting in lethality by E10.5-12.5. Mutants with remodeling failures are so common because normal development of the heart, blood and vessels is required for remodeling to occur. Our group has shown that vessel remodeling is regulated by hemodynamic force (physical forces exerted by flowing blood); thus, reduced circulation or lowered hematocrit (which reduces viscosity) can lead to remodeling failures (Lucitti et al., 2007). Moreover, endothelial cells (ECs) must respond to these signals, so if gene mutations alter early cardiac function (Huang et al., 2003; Koushik et al., 2001; Lucitti et al., 2007; May et al., 2004), lead to abnormal blood development (He et al., 2008) or disrupt normal EC development primarily (Graupera et al., 2008; Sengupta et al., 2012), then remodeling will fail as a secondary consequence. Also, pericardial edema and heart failure are consistently associated with yolk sac remodeling defects, regardless of the primary cause. This is probably because increasing the diameter of vessels is necessary to reduce the resistance that is encountered as blood circulates from the heart through the yolk sac. Thus, morphogenesis and function are very interdependent and crucial for survival.

Despite the importance of vessel remodeling for early development, little is known about the mechanisms that transform the initial capillary plexus into the vessel hierarchies that are evident by E9.5. Although it is clear that vessel remodeling is regulated by changes in hemodynamic force (Lucitti et al., 2007), it is unclear how such forces could alter the morphology and diameter of vessels. In mature vessels, where the endothelium is surrounded by contractile smooth muscle cells, blood flow can increase vessel diameter through muscle relaxation, but in the embryo smooth muscle cells are not detected surrounding vessels until after E9.5, when changes in diameter are already evident (Armstrong et al., 2010). This suggests that changes in diameter are likely to be regulated directly at the level of the EC.

Inspired by the work of Thoma (Thoma, 1893), who first proposed that blood circulation could regulate vessel morphogenesis, numerous studies have investigated the effects of shear stress and pressure on ECs (Califano and Reinhart-King, 2010; Chiu and Chien, 2011; Culver and Dickinson, 2010; Hahn and Schwartz, 2009; Li et al., 2005). Within the embryo, shear stress levels have been estimated to be ~5 dyn/cm^2 (Jones et al., 2004). Such low, oscillatory shear levels have been implicated in regulating cell proliferation, apoptosis and migration associated with the formation of atherosclerotic plaques (Chatzizisis et al., 2007; Chiu and Chien, 2011; Davies et al., 1986; Tardy et al., 1997; Tricot et al., 2000), and recent reports have shown that low-shear, interstitial flows can regulate endothelial sprouting, lymphangiogenesis and the migration of tumor and mesenchymal cells (Coffindaffer-Wilson et al., 2011; Haessler et al., 2012; Polacheck et al., 2011; Song and Munn, 2011; Yuan et al., 2012). These studies suggested that blood flow might regulate *in vivo* vessel

Department of Molecular Physiology and Biophysics, Baylor College of Medicine, Houston, TX 77030, USA.

*Author for correspondence (mdickins@bcm.tmc.edu)

Accepted 17 July 2013

remodeling in the mammalian yolk sac by regulating events such as EC proliferation, apoptosis or migration.

To test the hypothesis that blood flow regulates dynamic events in ECs such as proliferation, apoptosis or migration, we performed time-lapse confocal microscopy to visualize changes in EC behavior during remodeling. We used transgenic mice that fluorescently label the EC membranes (*Flk1-myr::mCherry*) and nuclei (*Flk1-H2B::eYFP*) and that label primitive blood cells (*ε-Globin-GFP*) (Dyer et al., 2001; Fraser et al., 2005; Larina et al., 2009; Poché et al., 2009). Using time-lapse imaging of dynamic events, as well as the analysis of cell death and proliferation in fixed embryos, we have found that vessel diameter increases do not result from changes in EC proliferation or survival. Instead, we show that diameter increases during vessel remodeling result from two different processes that are regulated by blood flow: vessel fusions near the vitelline artery and vein; and the directed migration of ECs from small to large vessels and within growing artery segments. These studies provide a clear view of the cellular behaviors that underlie vessel remodeling and answer longstanding questions about how forces from blood flow act on individual ECs during development.

MATERIALS AND METHODS

Mouse lines

Flk1-myr::mCherry (Larina et al., 2009; Poché et al., 2009) and *Flk1-H2B::eYFP* (Fraser et al., 2005; Larina et al., 2009) transgenic embryos were used for imaging experiments. For reduced flow experiments, myosin light chain 2 alpha$^{+/-}$ (*Mlc2a*$^{+/-}$); *Flk1-myr::mCherry*$^{tg/tg}$; *Flk1-H2B::eYFP*$^{tg/tg}$ mice were crossed to obtain *Mlc2a*$^{-/-}$ embryos that were labeled with EC markers (Huang et al., 2003; Lucitti et al., 2007). Embryos were genotyped using the following primers (5′-3′): mutant band, *Mlc2a*-mut-F (ACAGGGAATCACACCACCAT) and *Mlc2a*-mut-R (CGAACC-TGGTCGAAATCAG); wild-type band, *Mlc2a*-wt-F (GGCACGAT-CACTCAGTCAGA) and *Mlc2a*-wt-R (ATCCCTGTTCTGGTCAATGC). *ε-Globin-GFP* embryos (Dyer et al., 2001) were used to track GFP-labeled primitive erythroblasts for blood flow analysis. Ethical conduct was practiced with all mice following the IACUC-approved animal research protocols.

Determination of EC number per vessel diameter

To count ECs, *Flk1-myr::mCherry*$^{tg/tg}$; *Flk1-H2B::eYFP*$^{tg/tg}$ yolk sacs from E8.25 (~4-8 somites), E9.5 (21-29 somites) and E10.5 embryos were isolated, fixed in paraformaldehyde, flat mounted, and imaged on a Zeiss LSM 5 LIVE confocal microscope using a Plan-Neofluar 25×/0.8 objective. Total ECs (eYFP-labeled nuclei) were counted per vessel segment, where vessel boundaries were delineated before each branch point. Since each vessel segment is composed of distinct diameters and lengths, the number of ECs per vessel diameter was determined by extrapolating values using a fixed vessel length (200 μm). EC density was determined by quantifying the number of ECs per vessel segment surface area [number of ECs/(vessel diameter × vessel length × π)]. Statistical tests were performed in Microsoft Excel or MATLAB (MathWorks).

Immunohistochemistry

For immunostaining, yolk sacs were prepared as described (Lucitti et al., 2007). Primary antibodies used were rabbit anti-mouse phospho-histone H3 (PH3) (1:100; Millipore, #06-570), which labels mitotic cells, and rabbit anti-mouse cleaved caspase 3 (1:100; Cell Signaling, #9661), which labels apoptotic cells. Secondary antibodies were goat anti-rabbit IgG conjugated with Alexa Fluor 633 (Invitrogen, #21071).

Quantification of proliferative and apoptotic index

The proliferative and apoptotic indices were determined by counting the total number of PH3$^+$ or cleaved caspase 3$^+$ ECs among total *Flk1-H2B::eYFP* ECs. E8.5 and E9.5 yolk sac vessels were evaluated from entire yolk sacs of wild-type (‘normal flow’) and *Mlc2a*$^{-/-}$ (‘reduced flow’) embryos. The FARSIGHT program was used to quantify total EC numbers by segmenting YFP-labeled nuclei. PH3$^+$ or cleaved caspase 3$^+$ ECs were counted manually. For mitotic index, three embryos were used for each genotype representing 60 fields of view per genotype. For the apoptotic index, an average of three embryos was used for each genotype representing an average of 24 fields of view per genotype.

Live imaging of whole embryos

E8.5 (8-12 somites) mouse embryos were prepared for live imaging as described (Udan and Dickinson, 2010). All live imaging experiments were carried out on a Zeiss LSM 5 LIVE confocal microscope, using a Plan-Neofluar 25×/0.8 objective, with an environmentally controlled chamber (5% CO_2/95% humidified air at 37°C). For time-lapse imaging, laser power was optimized for embryo viability and image quality of *Flk1-H2B::eYFP* and *Flk1-myr::mCherry* labeled vessels. Yolk sac vessels were imaged with three *z*-plane sections for both fluorophores every 6-8 minutes for up to 24 hours. Embryos were genotyped after the imaging session.

For blood flow analysis, *ε-Globin-GFP* mice were imaged at ~216 Hz (one frame every 4.63 mseconds) and blood flow was assessed in proximal arteries, proximal veins and distal capillaries for 1.4 seconds each. Individual blood cells were tracked using Imaris (Bitplane) to obtain velocity profiles and flow patterns.

Cleavage orientation distribution

Analysis of the orientation of mitotic divisions was performed using time-lapse movies from wild-type and *Mlc2a*$^{-/-}$ embryos. The angle of EC division relative to the long axis of the vessel was determined for each mitotic event, and the distribution of the angles of EC divisions was plotted. ECs that underwent mitosis at the exact junctions between two vessels were omitted, as the axis of the vessel cannot be determined.

Computational analysis of cell migratory properties

EC migrations were evaluated from time-lapse movies of *Mlc2a*$^{+/+}$ and *Mlc2a*$^{-/-}$ embryos in proximal arteries and/or in specific vessels: low-flow vessel (LFV), <1000 μm/second peak blood velocities and low hematocrit; low-flow vessels interconnected to high-flow vessels (LFV-HFV); and high-flow vessel (HFV), ≤1500 μm/second blood velocities and high hematocrit. Cell migratory properties [total track length, total distance displaced, and tortuosity (total distance displaced divided by total track length)] were assessed using Imaris. Nuclei were tracked from frame to frame and the data were analyzed using Microsoft Excel. The migratory properties per vessel location were averaged, graphically represented in columns, and *t*-tests were performed to determine the statistical significance of cell movements between specific vessel locations and genotypes. The average difference in displacement track angles (see Results) was determined using Excel, and a nonlinear regression of the frequency of angles relative to the high-flow region was performed using Sigma Plot 10.

RESULTS

Remodeling results in larger diameter vessels composed of a greater number of ECs

Flk1-H2B::YFP and *Flk1-myr::mCherry* (*Flk1* is also known as *Kdr* – Mouse Genome Informatics) transgenic mice were used to examine changes in vessel architecture and EC composition in E8.5 (before remodeling) and E9.5 (during remodeling) embryos (Fig. 1A-D). The E8.5 primitive capillary plexus ranged in diameter from 10-90 μm (45 μm average) (Fig. 1A-B,E). E9.5 yolk sac vessels are arranged as a hierarchically branched tree with larger diameter (150-230 μm) vessels closest to the vitelline vein and artery, gradually leading to smaller diameter vessels (as small as 6 μm in diameter) distally (Fig. 1C-E). At this stage, the arterial tree comprises well-defined primary, secondary and tertiary branches, whereas the venous tree is composed of two dominant main vessels interconnected with many similar-sized vessels (Fig. 1C,D). Despite these differences, both sides remodel to establish hierarchical tree structures with the greatest diameter vessels most proximal to the vitelline artery and vein (referred to subsequently as the proximal arteries and veins; Fig. 1A-D).

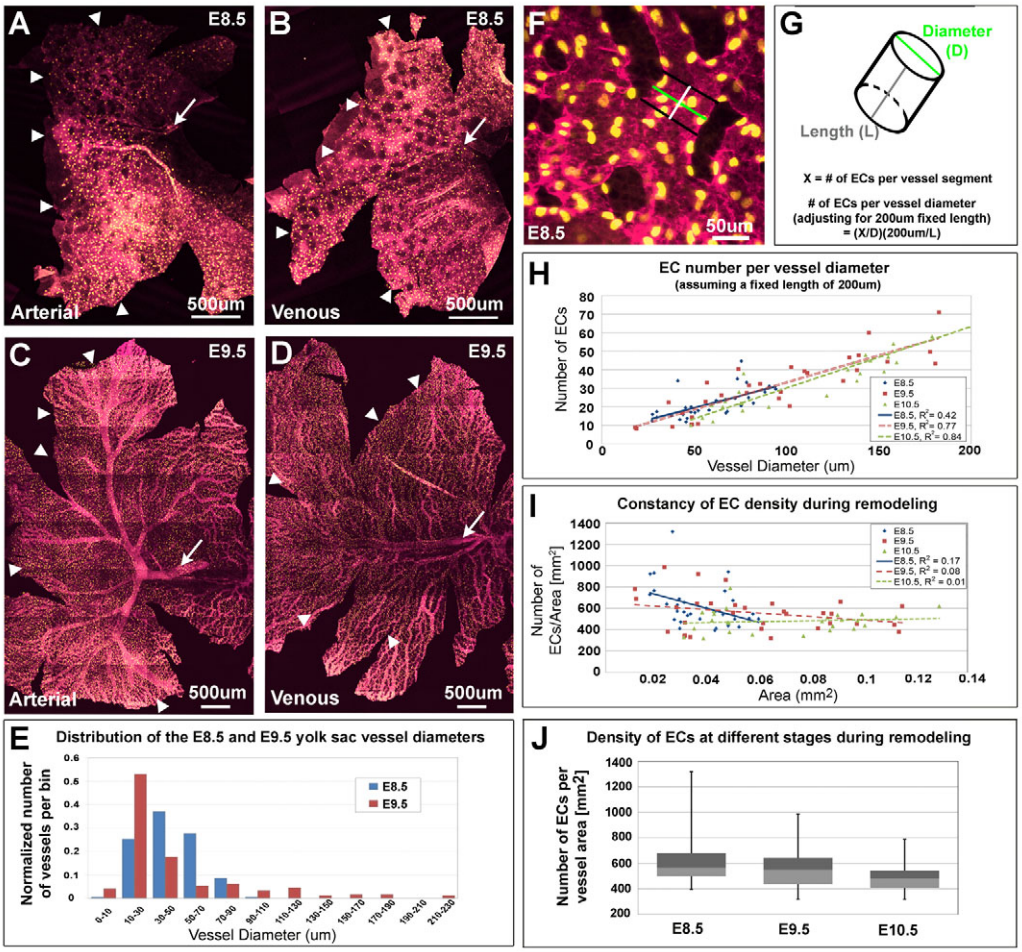

Fig. 1. Relationship between the number of endothelial cells and vessel diameter. (**A-E**) *Flk1-myr::mCherry* (magenta) and *Flk1-H2B::eYFP* (yellow) labeled vessels from flat-mounted E8.5 (A,B) and E9.5 (C,D) yolk sacs, with the distribution of vessel diameters at each stage (E). Proximal vessels (arrow) feed into distal vessels (arrowheads) (A-D). (**F**,**G**) The number of ECs per vessel diameter was measured by counting the number of YFP nuclei in a vessel segment. Vessel segment length [F, white bar (51.0 µm) or G, gray bar], diameter [F,G, green bar (81.96 µm)] and EC number were measured, and comparisons between EC number and diameter were made by adjusting the number of ECs per diameter vessel to a fixed vessel length (200 µm) (G). (**H**) The number of ECs per vessel diameter from E8.5, E9.5 and E10.5 yolk sacs (n=89 vessels from nine E8.5-10.5 mouse embryos). Trendlines represent best fits of the data. (**I**) EC density [number of ECs/area (mm^2)] versus area (mm^2) indicates no correlation between density and vessel segment area at any stage (R^2 values are close to 0). (**J**) Box plots of density measurements evaluated at different stages show similar median values [line between lower quartile (light gray) and upper quartile (dark gray)] at E8.5 and E9.5, but the median is slightly decreased at E10.5. A significant difference in the variance (difference between the lower and upper extremes) was also detected between stages, as indicated in the text.

To determine whether larger diameter vessels contain more ECs or have the same number of cells but differ in surface area, we examined the relationship between EC number and vessel diameter. The number of ECs per fixed length of vessel (200 µm) was counted in different diameter vessels of E8.5 to E10.5 yolk sacs (Fig. 1F,G). On average there was a greater investment of ECs concomitant with increasing vessel diameter (Fig. 1H), indicating that vessel enlargement is driven by increasing the number of ECs. The linear relationship between the average number of ECs and vessel diameter suggests that EC density is maintained as vessels remodel.

We analyzed the density directly (number of ECs per vessel surface area) and indeed found that density was constant, as we did not observe a dependence on the vessel segment area at any given embryonic stage (Fig. 1I). However, an analysis of the variance of the density values from E8.5-10.5 showed a decrease in variance at later stages (Fig. 1J; P=0.004, Bartlett test), perhaps as a response to vessel stabilization or to smooth muscle cell investment (Armstrong et al., 2010). We also observed a slightly lower median value at E10.5 (P=0.0081, Kruskal-Wallis test; Fig. 1J), which could indicate that vessels can stretch at later stages. However, it is unlikely that stretch plays a significant role during the E8.5 to E9.5 transition when the initial changes in diameter are established. If one compares ECs from large vessels (>80 µm) with ECs in small vessels (<40 µm), there is a slight but significant decrease in the average EC density (by 30%), indicating some possible stretch (data not shown). However, such a slight difference is insufficient to explain vessels that expand from 70-90 µm at E8.5 to diameters of 210-230 µm at E9.5 (2.75-fold increase). Rather, these data support the conclusion that increases in EC numbers underlie diameter expansion during remodeling.

EC proliferation and survival are not regulated by blood flow

Since viscous forces generated by blood flow (referred to herein as hemodynamic force or forces derived from blood flow) are required

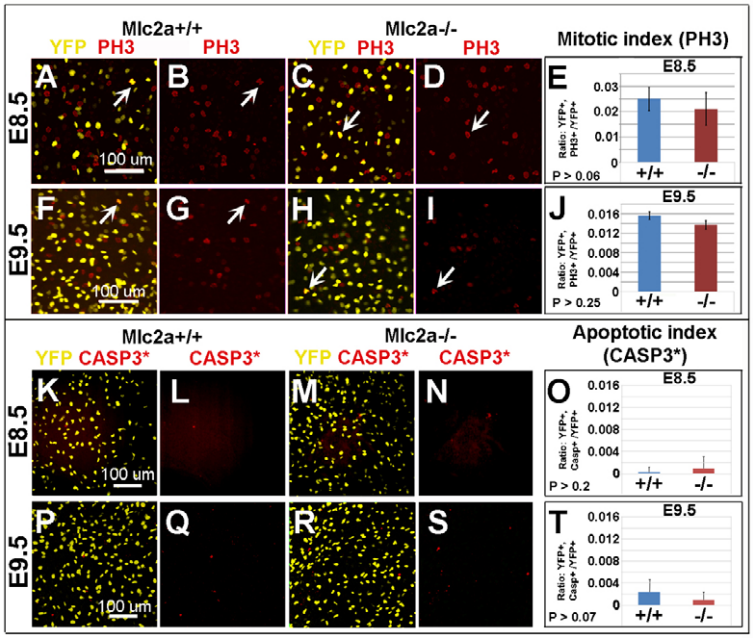

Fig. 2. Quantification of the mitotic and apoptotic indices of ECs in normal flow and reduced flow yolk sac vasculature. The number of phospho-histone H3 (PH3)-positive cells or the number of cleaved caspase 3-positive cells that colabeled (arrows) with *Flk1-H2B::eYFP* were counted in normal flow (*Mlc2a*$^{+/+}$) and reduced flow (*Mlc2a*$^{-/-}$) mouse embryos at E8.5 (**A-D** or **K-N**) and E9.5 (**F-I** or **P-S**). The mitotic index (**E**,**J**) or apoptotic index (**O**,**T**) was determined at E8.5 and E9.5 by counting the total number of PH3-positive or cleaved caspase 3-positive ECs among total ECs. Error bars represent s.d. For the mitotic index, *n*=3 yolk sacs per stage and per genotype, with a total of 20 fields of view per yolk sac. For the apoptotic index, *n*=3 yolk sacs per stage and per genotype, with a total of eight fields of view per yolk sac.

to promote vessel diameter increase (Lucitti et al., 2007), we sought to determine whether blood flow promotes EC proliferation in yolk sac vessels to increase diameter. EC proliferation was compared between wild-type and *Mlc2a*$^{-/-}$ [reduced blood flow (Huang et al., 2003; Lucitti et al., 2007)] yolk sacs during remodeling stages (*Mlc2a* is also known as *Myl7* – Mouse Genome Informatics). Immunochemistry was used to assess phospho-histone H3 (PH3) occurrence among *Flk1-H2B::eYFP* ECs to define the percentage of ECs undergoing mitosis (Fig. 2A-J). There was no statistically significant difference (*t*-test) in the EC mitotic index at either E8.5 (~8 somites; *P*=0.06) or E9.5 (~21 somites; *P*=0.25) between wild-type and *Mlc2a*$^{-/-}$ yolk sacs (Fig. 2E,J). Thus, EC proliferation does not appear to be influenced by blood flow or to be altered when remodeling fails in these embryos.

Alterations in EC survival could lead to an increased number of ECs in growing vessels if a high rate of apoptosis was present throughout the vasculature but was reduced in expanding vessels. We tested this by counting the percentage of ECs that are positive for cleaved caspase 3 (Fig. 2K-T). Both wild-type and *Mlc2a*$^{-/-}$ yolk sacs at E8.5 and E9.5 had very few cleaved caspase 3-positive ECs and there was no significant difference in the apoptotic index between the different genotypes (Fig. 2O,T).

The analysis of cell proliferation and apoptosis in fixed samples showed that there was no discernible difference in total dividing or dying cells that could account for diameter changes, but it was still possible that the fixed data somehow underestimated cell division or apoptosis rates. Also, previous studies of ECs *in vitro* have suggested that vessel diameter could be altered if ECs divide tangential to the vessel, adding cells to the width, rather than perpendicular to the vessel, adding to the length (Zeng et al., 2007). To address these possibilities, we analyzed confocal time-lapse sequences of E8.5-8.75 *Flk1-myr::mCherry* and *Flk1-H2B::eYFP* transgenic embryos grown in culture for 24 hours. These markers provide a direct, live assessment of changes in vascular architecture, EC division (Fig. 3A-C; mitotic separation of YFP-labeled nuclei), apoptosis (fragmentation of YFP-labeled nuclei) and cell migration (see below). Fig. 3 shows data obtained from imaging the proximal arterial side of the yolk sac, as this region shows the largest change in diameter during remodeling (Fig. 1A,C, arrow). In agreement with results shown in Fig. 2, imaging data from wild-type and *Mlc2a*$^{-/-}$ embryos exhibited no significant difference in the rate of EC mitosis or apoptosis (Fig. 3D). Further, analysis of the orientation of mitotic divisions showed that mitosis primarily occurred perpendicular to the cross-section of the vessel both in mutants and controls (Fig. 3E). Thus, the orientation of EC divisions was not influenced by flow, and if the mitotic plane influences vessel morphology then EC divisions would be likely to contribute to vessel length and not to vessel diameter (Zeng et al., 2007). Taken together, these data indicate that hemodynamic force does not drive increases in vessel size by altering the proliferation, survival or the orientation of mitosis of ECs.

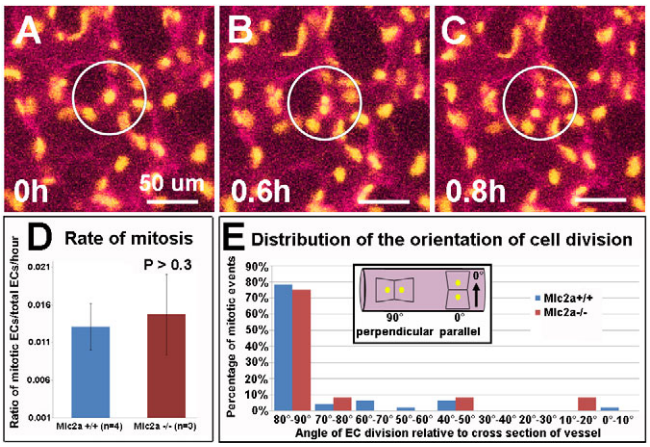

Fig. 3. Live imaging to quantify the orientation of cell divisions and mitotic indices in *Mlc2a*$^{+/+}$ versus *Mlc2a*$^{-/-}$ vessels. (**A-C**) Time-lapse movies of *Flk1-myr::mCherry* (magenta) and *Flk1-H2B::eYFP* (yellow) labeled vessels capture mitotic events that take place over 0-0.8 hours (separation of YFP-labeled nuclei, circled). (**D**) The mitotic index (number of mitotic events/average number of ECs per movie)/(time of EC in mitosis/total time of movie) was determined from *Mlc2a*$^{+/+}$ and *Mlc2a*$^{-/-}$ movies, and no statistically significant difference in the rate of mitosis was observed (*P*>0.3, *t*-test). Error bars indicate s.d. (**E**) The distribution of the angles of EC division, relative to the cross-section of the vessel (0°, arrow in inset), was plotted in *Mlc2a*$^{-/-}$ and *Mlc2a*$^{+/+}$ vessels from time-lapse movies.

Live imaging reveals segment fusions as vessels increase in diameter

Although proliferation, apoptosis and the orientation of mitotic divisions were not related to diameter changes, time-lapse movies did reveal specific dynamic events that contributed to increases in vessel diameter (supplementary material Movies 1-3). In the developing proximal arteries we detected segments of the capillary plexus fusing together, with an average of 2.75 fusion events per time-lapse sequence (Fig. 4A-D, white line; supplementary material Movies 1-3). Fusions eliminated the avascular space between neighboring vessels and occurred with the greatest frequency at around the 10-16 somite stage, after blood flow was established. By plotting changes in proximal artery diameter over time, it was apparent that fusion events resulted in a rapid increase in vessel diameter (Fig. 4E, red arrows; 40 μm increase). In addition to these abrupt changes, we also observed more incremental changes in vessel diameter occurring over longer time periods that did not coincide with vessel fusion (Fig. 4E). Thus, two different mechanisms might be at work to increase vessel diameter: a rapid change in diameter due to vessel fusion as well as a slower, more gradual process.

Because vessel fusion events occurred shortly after blood flow began, we examined whether vessel fusions could be detected in *Mlc2a*$^{-/-}$*; Flk1-H2B::YFP; Flk1-myr::mCherry* embryos with reduced blood flow. An analysis of at least three time-lapse sequences per mutant embryo revealed that fusion events were extremely rare in *Mlc2a*$^{-/-}$ embryos – only one fusion event appeared to initiate, but ultimately failed (Fig. 4F-J; supplementary material Movie 4). Instead, vessel diameter narrowed in these embryos as the surface area of the yolk sac increased (Fig. 4J). We next determined whether fusion events could be detected in capillary regions that do not increase in diameter and are exposed to lower flow. Imaging sequences confirmed, as expected, that capillaries in regions distant from the proximal vessels did not undergo fusion and the capillary diameter remained constant (Fig. 4K-O; supplementary material Movie 6). Finally, we examined time-lapse sequences taken near the vitelline vein and found that vessel fusion events did occur (note the loss of the avascular space;

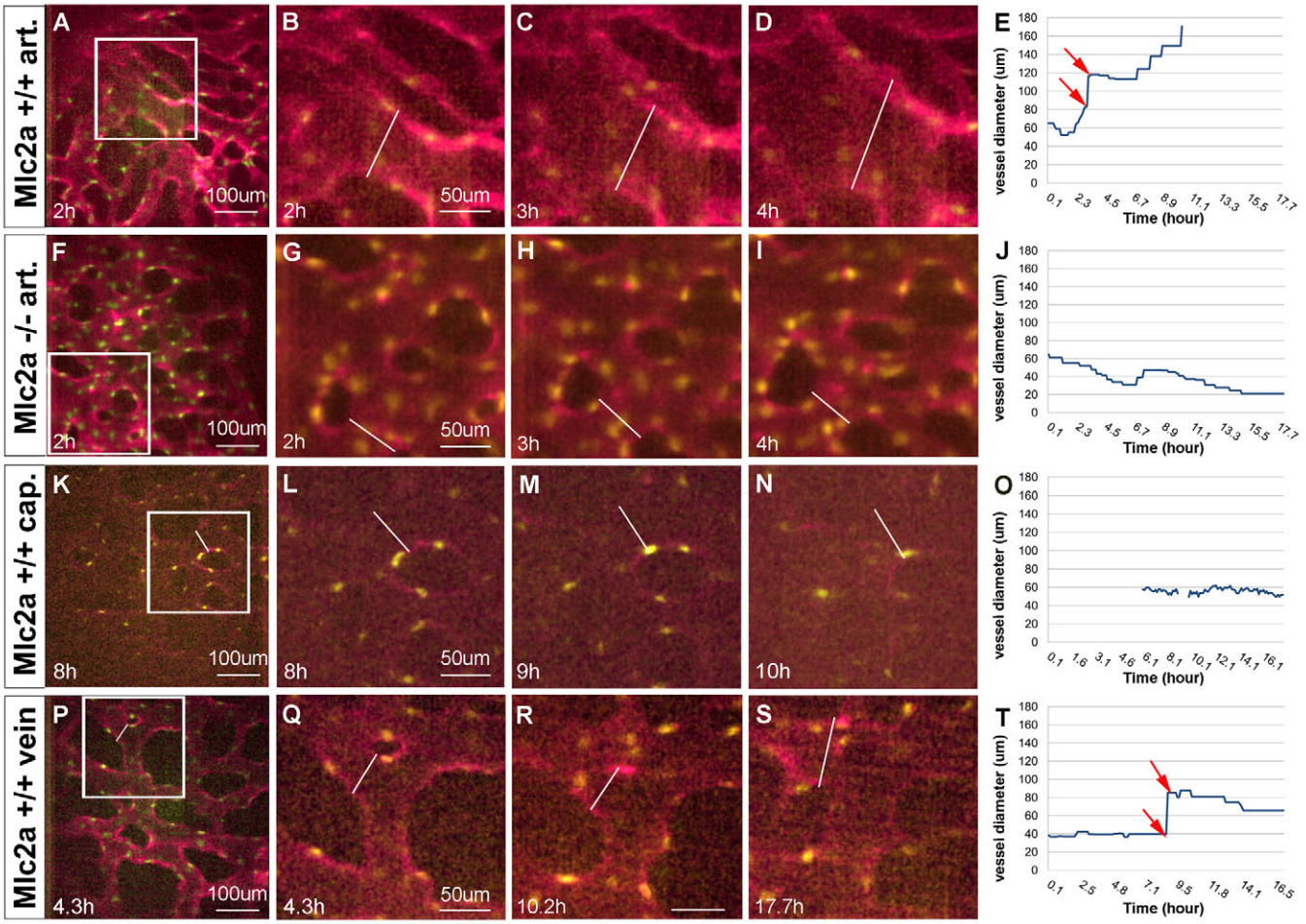

Fig. 4. Time-lapse analysis of changes in vessel diameter. Time-lapse movie sequences (starting at E8.5) of *Flk1-myr::mCherry; Flk1-H2B::eYFP* labeled ECs from *Mlc2a*$^{+/+}$ proximal arteries (**A-D**), *Mlc2a*$^{-/-}$ proximal arteries (**F-I**), *Mlc2a*$^{+/+}$ distal capillaries (**K-N**) and *Mlc2a*$^{+/+}$ proximal veins (**P-S**). Detail of the boxed regions in A, F, K and P are shown for select time-lapse sequences. Changes in vessel diameters (white bar) are displayed graphically over time (**E**,**J**,**O**,**T**). Rapid changes in vessel diameters (red arrows) were coincident with the fusion of two neighboring vessels and the loss of an avascular space between them, as in the *Mlc2a*$^{+/+}$ proximal artery (A-D) or the *Mlc2a*$^{+/+}$ proximal vein (P-S), but such rapid changes were not seen in *Mlc2a*$^{-/-}$ vessels (F-I) or *Mlc2a*$^{+/+}$ distal capillaries (K-N). A slower rate of change was also observed during *Mlc2a*$^{+/+}$ proximal artery remodeling, as there was a steady rate of diameter increase in addition to the rapid change associated with fusions (A-D). This was not observed in other groups that either exhibited reduced vessel growth (*Mlc2a*$^{-/-}$ vessels, F-I), no net change in diameter (*Mlc2a*$^{+/+}$ distal capillaries, K-N) or where the only diameter increase that occurred correlated with the fusion event (*Mlc2a*$^{+/+}$ proximal vein, P-S).

Fig. 4P-S, white line; 4T, red arrows; supplementary material Movie 5). In the example shown in Fig. 4P-S, fusion led directly to a rapid increase in diameter (arrow) that was stable for several hours, but the vessel did not expand further during this session.

Together, these data show that vessel fusion events occur in both veins and arteries and lead to significant increases in diameter, but are absent in capillaries and low-flow vessels.

Regions of the yolk sac vasculature prone to vessel fusion experience the highest blood flow velocities

Because blood flow is known to induce changes in remodeling (Lucitti et al., 2007), and both the distal capillaries and *Mlc2a*$^{-/-}$ yolk sac vessels do not undergo fusion, we directly examined temporal changes in the flow velocity profile in different regions of the yolk sac to determine whether fusion events correlate with flow velocity or pulsatility.

In E8.25 (~6 somites) embryos, vessel diameters were relatively similar in size (averaging ~45 μm in diameter) and have yet to remodel. Peak blood velocities were highest in proximal arteries (~2000 μm/second) when compared with the flow in proximal veins (~1000 μm/second) and distal capillaries (~600 μm/second) (Fig. 5A-C). In E8.75 embryos (~12 somites), peak blood velocities increased in proximal arteries and slightly increased in proximal veins, but were more variable in capillaries (Fig. 5D-F). This variation was caused by the preferred path of blood flow, whereby some distal capillaries were connected to more direct paths of blood flow than others, resulting in a wide range of peak blood velocities in 12-somite capillaries (<1000 to ~1200 μm/second). By E9.5 (21 somites), proximal arteries maintained a sharp pulsatility with high maximum velocities (~5500 μm/second; Fig. 5G-I). However, the pulsatility of blood flow in proximal veins was less distinct and more continuous, with maximum velocities at ~1500 μm/second (Fig. 5I). Distal capillaries that had a less direct path of blood flow exhibited the weakest peak blood velocities (~900 μm/second; Fig. 5H).

Comparing the blood flow analysis with the time-lapse data, vessel fusion events were detected shortly after flow began (~E8.5-9.0) in the most proximal vessels, where strong pulsatile flows were found relative to more distal capillaries, suggesting that fusions occur in response to the highest magnitude flows.

Changes in arterial diameter are associated with EC migration and recruitment

Analysis of the changes in vessel diameter over time suggested that, in addition to vessel fusion, there was also a slower event that promotes vessel diameter increase (Fig. 4D). To identify these events, EC migration was analyzed in time-lapse movies using the *Flk1-H2B::YFP; Flk1-myr::mCherry* markers. EC migration tracks were examined in the proximal arterial region of wild-type embryos and *Mlc2a*$^{-/-}$ embryos with reduced flow, as well as in the low-flow capillaries and near the proximal vein of wild-type embryos.

YFP-labeled EC nuclei were highly dynamic and showed consistent migration behaviors during vascular remodeling (translocating up to 180 μm from their original position) (supplementary material Movies 1-3; Fig. 6A-D). During the expansion of vessels neighboring the proximal artery of wild-type yolk sacs, ECs were observed migrating from neighboring small, interconnected vessels towards larger artery segments (Fig. 6A-D, arrows). Intravessel EC migrations were also detected within growing vessels toward the more proximal region of the vessel and against the direction of blood flow (Fig. 6E-H). EC nuclei were not associated with angiogenic sprouts, and ECs were not observed

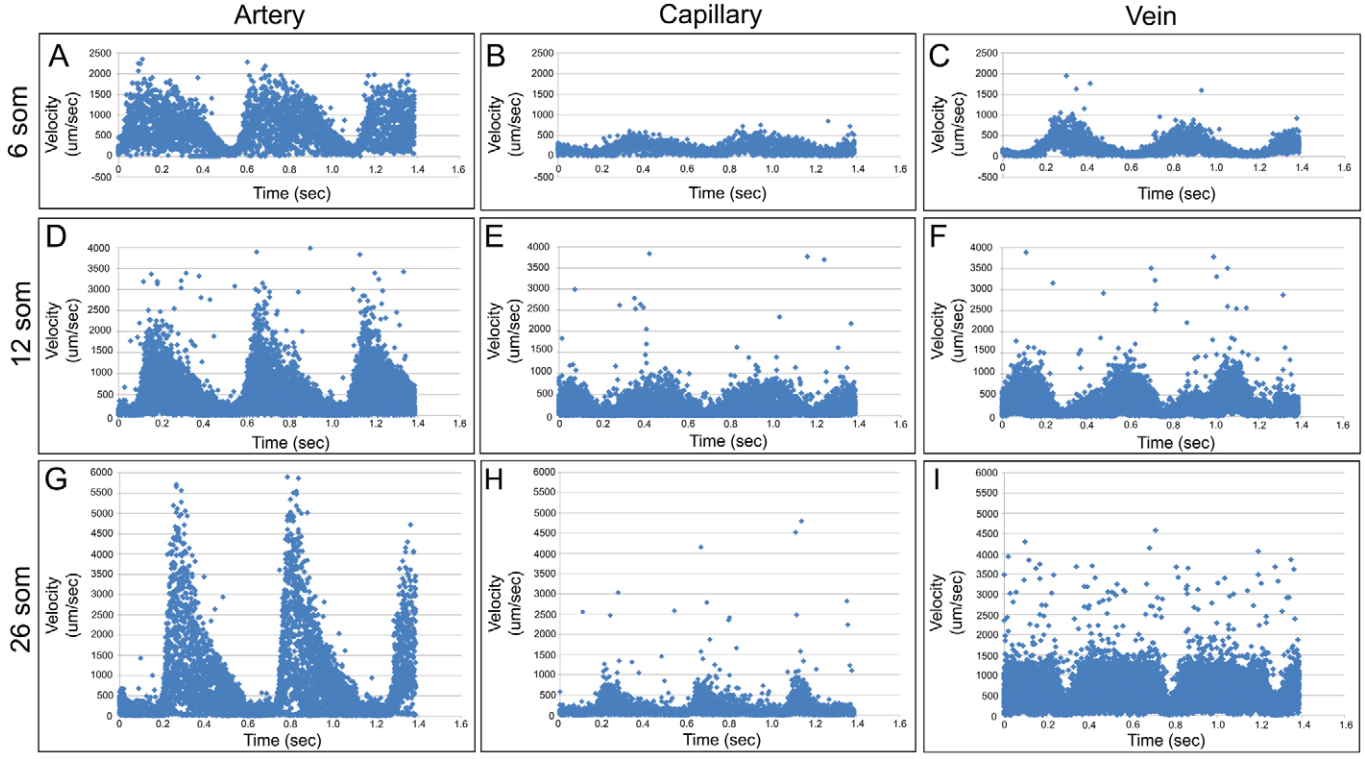

Fig. 5. Blood flow profiles at different stages of remodeling from developing arterial, venous and capillary vessels. Fast line-scan confocal imaging was used to track *ε-Globin-GFP* labeled erythrocytes to measure blood velocities in developing arterial and venous vessels. Blood velocities were plotted over time (~1.4 seconds) in developing arteries, capillaries and veins of late E8.25 (**A-C**), E8.75 (**D-F**) and E9.5 (**G-I**) mouse embryos.

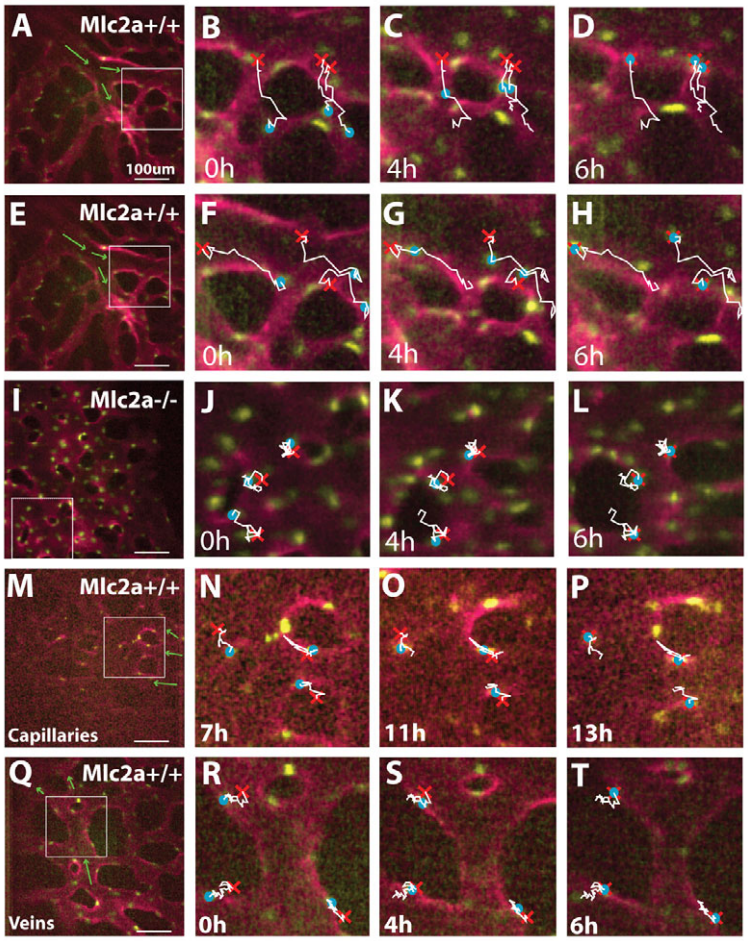

Fig. 6. ECs show regional differences in migration. Images from time-lapse sequences from 0, 4 or 6 hours after the start of the sequence, showing the continuous migration tracks (white lines) of selected ECs. The direction of blood flow is indicated by green arrows. Blue circles indicate the position of the tracked EC at the time of the frame of the time-lapse sequence, and the red 'X' indicates the end of each migration track. Tracks of ECs within the developing arteries of wild-type embryos showed migration from low-flow interconnected capillaries towards and into the growing arteries with high flow (**A-D**), and showed proximal migration within high-flow arteries (**E-H**). By contrast, migration tracks of ECs in the proximal arteries of *Mlc2a*$^{-/-}$ embryos (**I-L**), in wild-type capillaries (**M-P**) and in wild-type proximal veins (**Q-T**) did not appear to have a consistent direction or extend very far from the start position.

undergoing intravasation into the vessel lumen. Instead, ECs moved within or closely apposed to the endothelial wall of intact vessels (supplementary material Movie 1). Given these results, we expected that EC migration might be reduced or absent in *Mlc2a*$^{-/-}$ embryos. However, we observed significant EC cell motility, although ECs appeared to move in a random pattern and remained within 20 μm of their initial position (Fig. 6I-L; supplementary material Movie 4). Similar to results from *Mlc2a*$^{-/-}$ embryos, tracks of ECs in distal capillaries of wild-type embryos (low-flow regions; Fig. 5; supplementary material Movie 5) also showed active motility but no apparent directional migratory behavior (Fig. 6M-P). Lastly, we examined migration events in proximal veins. In contrast to migration near the vitelline artery, we did not observe directed migration. Venous ECs were motile but migration tracks were random and confined, similar to those in distal capillaries (Fig. 6Q-T; supplementary material Movie 6).

Non-random, directed EC migration toward regions of greater blood flow and expanding vessel diameter

The observations above suggested that the slow process of vessel diameter growth could result from the active recruitment of ECs to larger blood vessels in response to increased blood flow. To address this hypothesis, we performed a quantitative assessment of EC migration in time-lapse sequences to determine whether there was a consistent and significant relationship between EC migration and differences in blood flow. Four different scenarios related to blood flow (in order of lowest to highest blood flow) were analyzed: ECs in the low-flow proximal arteries of *Mlc2a*$^{-/-}$ embryos [Fig. 7A; *Mlc2a*$^{-/-}$ LFV (low-flow vessel)]; ECs in the low-flow/distal capillaries of *Mlc2a*$^{+/+}$ (wild-type) embryos (Fig. 7B; *Mlc2a*$^{+/+}$ LFV); ECs in capillaries connected to larger diameter/high-flow arteries in *Mlc2a*$^{+/+}$ embryos [Fig. 7C; *Mlc2a*$^{+/+}$ LFV-HFV (low-flow vessel connected to high-flow vessel)]; and ECs within expanding/high-flow arteries in *Mlc2a*$^{+/+}$ embryos [Fig. 7D; *Mlc2a*$^{+/+}$ HFV (high-flow vessel)]. To determine whether the extent of EC migration was influenced by flow in these groups, we compared differences in the displacement of ECs [how far they travel from the beginning to end of the time-lapse sequence over time (μm/hour)], and the total length of the migration track per hour (Fig. 7E,F). No significant difference in the total displacement of ECs per unit time was observed between the *Mlc2a*$^{-/-}$ LFV and *Mlc2a*$^{+/+}$ LFV groups, or between the *Mlc2a*$^{+/+}$ LFV-HFV and *Mlc2a*$^{+/+}$ HFV groups; however, the average total displacement between ECs from the two low-flow categories was significantly less than that of the two high-flow categories (Fig. 7E). Thus, ECs within, or neighboring, regions of higher flow migrated significantly further from their original start position over time than ECs in low-flow regions. Interestingly, there was no significant difference between the average total track length per unit time between any of the groups (Fig. 7F). Thus, the ability to move or the duration of migration was not dictated by blood flow, but the total distance traveled was influenced by blood flow.

We then determined whether the migration paths of LFV ECs were more tortuous than those of LFV-HFV and HFV ECs. Tortuosity is the ratio of the displacement to total track length, so

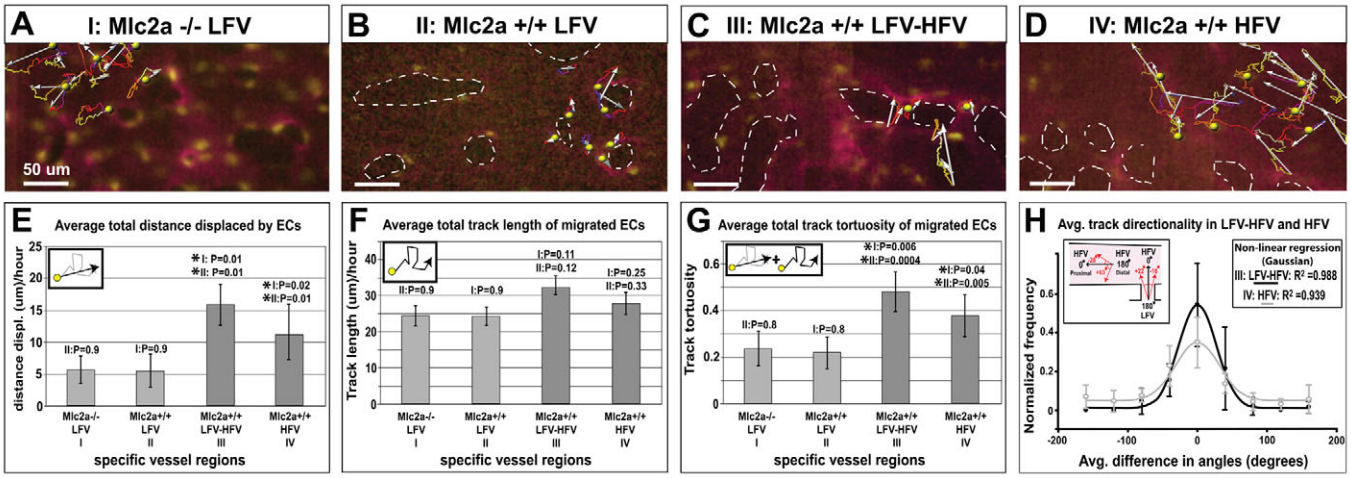

Fig. 7. ECs exhibit increased motility and directional migration in interconnected vessels adjacent to and within vessels of high flow. (**A-D**) EC tracks (colored lines) and displacement vectors (gray arrows) in selected arterial or capillary regions are shown for: (A) low-flow vessels (LFV) from *Mlc2a*$^{-/-}$ embryos (group I); (B) LFV from *Mlc2a*$^{+/+}$ embryos (group II); (C) low-flow vessels interconnected to high-flow vessels (LFV-HFV) from *Mlc2a*$^{+/+}$ embryos (group III); and (D) high-flow vessels (HFV) from *Mlc2a*$^{+/+}$ embryos (group IV). (**E-H**) Average total displacement (E), average total track length (F) and average tortuosity (G) of EC migration tracks were measured for each group. Significant differences in the average displacement and average tortuosity were seen for groups I/II compared with groups III/IV. Differences in the angles of EC displacement tracks, relative to the region of higher flow, are shown for groups III and IV in H. A non-linear regression was performed to demonstrate a Gaussian distribution for both groups. Error bars indicate s.d.

migration in a straight line would have a tortuosity of 1, whereas more tortuous paths would have values of less than 1. EC migrations in *Mlc2a*$^{-/-}$ LFVs and in *Mlc2a*$^{+/+}$ LFVs were found to be highly tortuous (Fig. 7G; mean tortuosity of 0.24±0.07 and 0.22±0.07, respectively). However, ECs migrating from LFV-HFVs and within HFVs showed less tortuous migrations (Fig. 7G; mean tortuosity of 0.49±0.08 and 0.38±0.09, respectively). These data show that ECs within and near regions that are actively remodeling in response to blood flow move in a less tortuous, more directed path.

The less tortuous migration tracks in the LFV-HFV and HFV categories could suggest that ECs were migrating towards a particular target or they could result from spatial confinement of ECs. To distinguish between these models, we first established an ideal trajectory in which a vector was drawn from the LFV to the HFV, or was drawn towards the larger end of the vessel in the HFV (Fig. 7H). Next, we determined the difference angle between the EC displacement vector and the idealized vector to establish whether ECs were aligned with the idealized vector. If ECs were undergoing directional migration to increase diameter, we would expect a 0° divergence from the idealized vector. If EC migrations were limited by spatial confinement, we would expect two peak divergences from the idealized vector (0° and 180°) because ECs could move towards or away from the idealized goal (the larger vessel). Our results revealed a Gaussian distribution, with a peak average difference in displacement angles at 0° for both the LFV-HFV and HFV scenarios (Fig. 7H, black and gray lines, respectively). ECs move towards the growing vessel preferentially, supporting the directed migration model. The LFV-HFV and HFV groups showed a significant difference in the maximum frequency of the distributions (0.54 and 0.35, respectively), indicating smaller angle differences because of smaller diameter LFV-HFVs as compared with HFVs. However, despite the confinement in migration angle, ECs showed a very strong preference for migration towards the larger diameter vessel in both cases. These data show that EC migration is oriented towards regions of greater flow to contribute to the change in vessel diameter.

DISCUSSION

High-resolution live imaging of cultured mouse embryos was used to elucidate the cellular events that underlie changes in vessel structure as the capillary plexus remodels into a hierarchical vessel tree. Using EC-specific fluorescent protein reporters to track EC changes during normal remodeling and during remodeling failure, when flow is impaired, showed that vessel remodeling is not driven by changes in cell proliferation or cell death or the orientation of the cell division plane, but did reveal vessel fusion events and changes in cell migration that regulate vessel remodeling. Fig. 8 depicts the series of events that we have defined. Shortly after blood flow begins, blood flow circulates through the yolk sac with the strongest flows through the proximal arterial and venous regions. In response to such high levels of flow, and probably in response to considerable resistance by the small capillaries, fusions are induced between neighboring vessels causing a rapid change in vessel diameter in the proximal vessels of the tree (Fig. 8A). Concomitant with the first fusion events, ECs are recruited to the expanding arteries, migrating in a directed and persistent manner to support vessel growth (Fig. 8B). These two sets of events together transform the initially small capillaries into a pattern of larger vessels (Fig. 8C).

By directly examining dynamic changes in EC behavior during remodeling in both wild-type and *Mlc2a*$^{-/-}$ flow-deficient embryos, we concluded that vessel fusions, as well as directed cell migration, are triggered by blood flow. Although vessel fusions have been noted in a previous study of vessel remodeling in avian embryos (le Noble et al., 2004), the data presented here clearly show that vessel fusions are restricted to regions where there is strong, pulsatile flow – fusions are absent in capillaries or mutant yolk sacs when flow is reduced – and that fusions result in a rapid change in vessel diameter that establishes the proximalmost parent vessels of the vessel tree. Fusion events occur on both the early arterial and venous sides of the yolk sac, so these events do not seem to depend on flow direction or arterial-venous specification. However, since early proximal arteries and veins both have strong pulsatile flows, we could not distinguish whether the magnitude of the flows, the pulsatility or the resistance

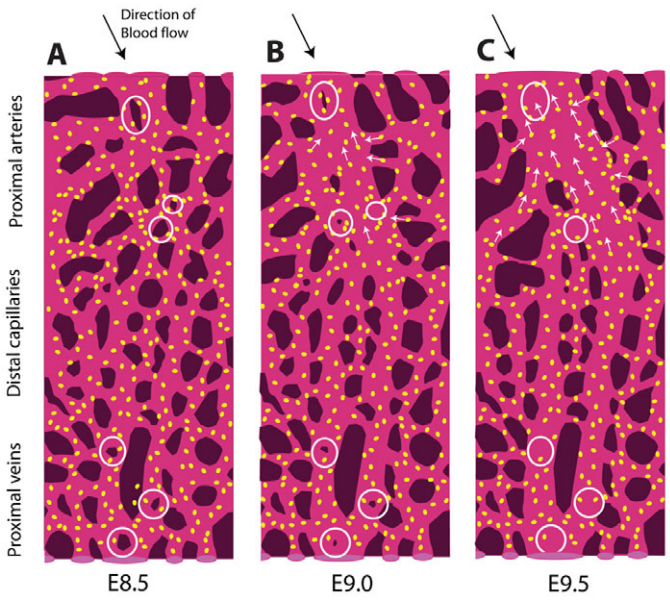

Fig. 8. Model of yolk sac vascular remodeling in response to changes in blood flow. (**A**) Blood enters the vascular plexus at E8.5 through the vitelline artery. In the proximal arterial region of the yolk sac, a randomly chosen, preferred path of flow forms. Blood is then diverted to the distal capillaries and is ultimately collected by the vitelline vein. Vessel remodeling occurs by the redistribution of ECs via vessel fusions (circles) and directed EC migrations (white arrows in B,C), resulting in a rapid and a slower change in vessel diameter, respectively. Proximal vessels that are exposed to high peak blood velocities and high resistances undergo vessel fusion (circles) with neighboring vessels. (**B**,**C**) By E9.0-9.5, fusions help to establish vessel hierarchy, resulting in proximal arteries with pulsatile/high velocity flows, distal capillaries with pulsatile/low velocity flows, and proximal veins with steadier/low velocity flows. The amount of force that is exhibited by these flow profiles correlates well with observed directed migrations that occur from low-flow vessels to high-flow/growing arteries, and upstream of flow in high-flow/growing arteries – events that are absent in distal capillaries and proximal veins. The unique responses that ECs exhibit in different regions might explain not only how vessel hierarchies form, but also how arterial and venous morphologies are established.

encountered by the small capillaries as blood enters the plexus was most important for inducing these events. As we did not detect significant stretch in these vessels, it is likely that they lack the extensibility to lessen the resistance encountered when blood enters the plexus. Thus, vessel fusion events might represent an efficient adaptation mechanism for reducing resistance.

It is not yet clear how vessel fusion events are regulated on a molecular level in the mouse yolk sac. Avian studies implicate VEGF in regulating the fusion of the bilateral dorsal aorta (Garriock et al., 2010), and ectopic activation of VEGF signaling in the avian chorioallantoic membrane resulted in an unremodeled but hyperfused vessel phenotype (Drake and Little, 1995). Similarly, mouse mutations in *Flt1* or *Ptprj* (*CD148*, *Dep1*) result in upregulation of *Vegf*, and mutants show large and unremodeled vessels (Argraves and Drake, 2005; Fong et al., 1999; Takahashi et al., 2003). Since VEGFR2 (Kdr) has been shown to be part of a force-sensing complex in ECs (Tzima et al., 2005), we attempted to block VEGF signaling during flow-induced remodeling using chemical inhibitors; however, this induced the death of ECs (R.S.U. and M.E.D., unpublished) and did not reveal a clear involvement of VEGF signaling in vessel fusions.

Directed EC migration events triggered by blood flow were also detected during vessel remodeling. ECs migrated upstream and against flow in growing arterial segments, and from low-flow capillaries to adjacent high-flow arteries. Similar anterograde migration events have been observed in the dorsal aorta in avian embryos (Sato et al., 2010), but here we show that these events are dependent on blood flow and contribute to the diameter changes needed for vessel remodeling. We did not detect significant directional migration on the venous side, nor did we observe a second, slow phase of vessel growth, although vessel fusions were detected on the venous side, producing rapid changes in vessel diameter (Fig. 4T). The presence of fusion events but the absence of directed migrations on the venous side might explain why vessel morphologies differ between the arterial and venous trees. For instance, arteries have a distinct hierarchical ramified tree comprising primary, secondary and tertiary main branches. Our data suggest that this more complex pattern in arteries results from both fusion and migration events, whereas the simpler pattern on the venous side, with two dominant vessels, is likely to result from fusions without subsequent migrations.

Although it is not yet clear how hemodynamic forces could promote EC recruitment, it is possible that ECs could be responding to a chemical signal released by cells experiencing force (i.e. chemotaxis) or that they are sensing graded differences in shear stress or substrate tension (i.e. mechanotaxis) (Chiu and Chien, 2011). However, regardless of whether chemotaxis or mechanotaxis is used, not all cells in the vessel migrate at once. Precisely how graded signals could be interpreted differently by neighboring cells is a challenging problem, but is reminiscent of cell fate decisions regulated by Notch pathways (Jakobsson et al., 2009; Roca and Adams, 2007). Since Notch factors are also key regulators of arterial-venous differentiation, it is possible that such a lateral inhibition mechanism could be involved in determining how some arterial cells can respond to flow by migrating directionally whereas other neighbors do not respond.

Previous studies have defined scaling relationships between parent and daughter vessels in vascular trees (Murray, 1926; Sherman, 1981) and have tested these principles using models that replicate changes during remodeling in embryos (Gödde and Kurz, 2001; Szczerba et al., 2009; Taber et al., 2001); however, these studies have only focused on the meso-scale pattern of vessels that emerges in response to blood flow. Here we have defined the micro-scale events that underlie how a simple, interconnected plexus can form an enlarged and elaborated vessel tree. In addition to elucidating the mechanisms that regulate this critical transition in mammalian development, these data also have implications for tissue engineering and repair strategies. Growing enlarged vessels from small capillary networks remains a key hurdle to engineering vascularized organs or tissues *in vitro* (Franco and Gerhardt, 2012; Nemeno-Guanzon et al., 2012; Zheng et al., 2012). The dynamic behaviors of ECs described here could provide important clues in the quest to generate *de novo* vessel structures that can undergo normal physiological remodeling.

Acknowledgements
We would like to acknowledge the BCM Optical Imaging and Vital Microscopy (OIVM) core.

Funding
National Institutes of Health: National Institute of General Medical Sciences [K12 GM084897] and National Heart Blood and Lung Institute [R01 HL097520, T32 HL07676 and R01 HL077187]; and the American Heart Association [10POST4280097]. Deposited in PMC for release after 12 months.

Competing interests statement
The authors declare no competing financial interests.

Author contributions
R.S.U., T.J.V. and M.E.D. contributed to the design of the research. R.S.U. and M.E.D. wrote the manuscript. T.J.V. contributed to experiments on EC number versus vessel diameter and to statistical analysis throughout. R.S.U. performed the experiments.

Supplementary material
Supplementary material available online at
http://dev.biologists.org/lookup/suppl/doi:10.1242/dev.096255/-/DC1

References

Argraves, W. S. and Drake, C. J. (2005). Genes critical to vasculogenesis as defined by systematic analysis of vascular defects in knockout mice. *Anat. Rec. A Discov. Mol. Cell. Evol. Biol.* **286**, 875-884.
Armstrong, J. J., Larina, I. V., Dickinson, M. E., Zimmer, W. E. and Hirschi, K. K. (2010). Characterization of bacterial artificial chromosome transgenic mice expressing mCherry fluorescent protein substituted for the murine smooth muscle alpha-actin gene. *Genesis* **48**, 457-463.
Califano, J. P. and Reinhart-King, C. A. (2010). Exogenous and endogenous force regulation of endothelial cell behavior. *J. Biomech.* **43**, 79-86.
Chatzizisis, Y. S., Coskun, A. U., Jonas, M., Edelman, E. R., Feldman, C. L. and Stone, P. H. (2007). Role of endothelial shear stress in the natural history of coronary atherosclerosis and vascular remodeling: molecular, cellular, and vascular behavior. *J. Am. Coll. Cardiol.* **49**, 2379-2393.
Chiu, J. J. and Chien, S. (2011). Effects of disturbed flow on vascular endothelium: pathophysiological basis and clinical perspectives. *Physiol. Rev.* **91**, 327-387.
Coffindaffer-Wilson, M., Craig, M. P. and Hove, J. R. (2011). Normal interstitial flow is critical for developmental lymphangiogenesis in the zebrafish. *Lymphat. Res. Biol.* **9**, 151-158.
Culver, J. C. and Dickinson, M. E. (2010). The effects of hemodynamic force on embryonic development. *Microcirculation* **17**, 164-178.
Davies, P. F., Remuzzi, A., Gordon, E. J., Dewey, C. F., Jr and Gimbrone, M. A., Jr (1986). Turbulent fluid shear stress induces vascular endothelial cell turnover in vitro. *Proc. Natl. Acad. Sci. USA* **83**, 2114-2117.
Drake, C. J. and Little, C. D. (1995). Exogenous vascular endothelial growth factor induces malformed and hyperfused vessels during embryonic neovascularization. *Proc. Natl. Acad. Sci. USA* **92**, 7657-7661.
Dyer, M. A., Farrington, S. M., Mohn, D., Munday, J. R. and Baron, M. H. (2001). Indian hedgehog activates hematopoiesis and vasculogenesis and can respecify prospective neurectodermal cell fate in the mouse embryo. *Development* **128**, 1717-1730.
Fong, G. H., Zhang, L., Bryce, D. M. and Peng, J. (1999). Increased hemangioblast commitment, not vascular disorganization, is the primary defect in flt-1 knock-out mice. *Development* **126**, 3015-3025.
Franco, C. and Gerhardt, H. (2012). Tissue engineering: blood vessels on a chip. *Nature* **488**, 465-466.
Fraser, S. T., Hadjantonakis, A. K., Sahr, K. E., Willey, S., Kelly, O. G., Jones, E. A., Dickinson, M. E. and Baron, M. H. (2005). Using a histone yellow fluorescent protein fusion for tagging and tracking endothelial cells in ES cells and mice. *Genesis* **42**, 162-171.
Garriock, R. J., Czeisler, C., Ishii, Y., Navetta, A. M. and Mikawa, T. (2010). An anteroposterior wave of vascular inhibitor downregulation signals aortae fusion along the embryonic midline axis. *Development* **137**, 3697-3706.
Gödde, R. and Kurz, H. (2001). Structural and biophysical simulation of angiogenesis and vascular remodeling. *Dev. Dyn.* **220**, 387-401.
Graupera, M., Guillermet-Guibert, J., Foukas, L. C., Phng, L. K., Cain, R. J., Salpekar, A., Pearce, W., Meek, S., Millan, J., Cutillas, P. R. et al. (2008). Angiogenesis selectively requires the p110alpha isoform of PI3K to control endothelial cell migration. *Nature* **453**, 662-666.
Haessler, U., Teo, J. C., Foretay, D., Renaud, P. and Swartz, M. A. (2012). Migration dynamics of breast cancer cells in a tunable 3D interstitial flow chamber. *Integr. Biol. (Camb.)* **4**, 401-409.
Hahn, C. and Schwartz, M. A. (2009). Mechanotransduction in vascular physiology and atherogenesis. *Nat. Rev. Mol. Cell Biol.* **10**, 53-62.
He, C., Hu, H., Braren, R., Fong, S. Y., Trumpp, A., Carlson, T. R. and Wang, R. A. (2008). c-myc in the hematopoietic lineage is crucial for its angiogenic function in the mouse embryo. *Development* **135**, 2467-2477.
Huang, C., Sheikh, F., Hollander, M., Cai, C., Becker, D., Chu, P. H., Evans, S. and Chen, J. (2003). Embryonic atrial function is essential for mouse embryogenesis, cardiac morphogenesis and angiogenesis. *Development* **130**, 6111-6119.
Jakobsson, L., Bentley, K. and Gerhardt, H. (2009). VEGFRs and Notch: a dynamic collaboration in vascular patterning. *Biochem. Soc. Trans.* **37**, 1233-1236.
Jones, E. A., Baron, M. H., Fraser, S. E. and Dickinson, M. E. (2004). Measuring hemodynamic changes during mammalian development. *Am. J. Physiol.* **287**, H1561-H1569.
Koushik, S. V., Wang, J., Rogers, R., Moskophidis, D., Lambert, N. A., Creazzo, T. L. and Conway, S. J. (2001). Targeted inactivation of the sodium-calcium exchanger (Ncx1) results in the lack of a heartbeat and abnormal myofibrillar organization. *FASEB J.* **15**, 1209-1211.
Larina, I. V., Shen, W., Kelly, O. G., Hadjantonakis, A. K., Baron, M. H. and Dickinson, M. E. (2009). A membrane associated mCherry fluorescent reporter line for studying vascular remodeling and cardiac function during murine embryonic development. *Anat. Rec. (Hoboken)* **292**, 333-341.
le Noble, F., Moyon, D., Pardanaud, L., Yuan, L., Djonov, V., Matthijsen, R., Bréant, C., Fleury, V. and Eichmann, A. (2004). Flow regulates arterial-venous differentiation in the chick embryo yolk sac. *Development* **131**, 361-375.
Li, Y. S., Haga, J. H. and Chien, S. (2005). Molecular basis of the effects of shear stress on vascular endothelial cells. *J. Biomech.* **38**, 1949-1971.
Lucitti, J. L., Jones, E. A., Huang, C., Chen, J., Fraser, S. E. and Dickinson, M. E. (2007). Vascular remodeling of the mouse yolk sac requires hemodynamic force. *Development* **134**, 3317-3326.
May, S. R., Stewart, N. J., Chang, W. and Peterson, A. S. (2004). A Titin mutation defines roles for circulation in endothelial morphogenesis. *Dev. Biol.* **270**, 31-46.
Murray, C. D. (1926). The physiological principle of minimum work: I. the vascular system and the cost of blood volume. *Proc. Natl. Acad. Sci. USA* **12**, 207-214.
Nemeno-Guanzon, J. G., Lee, S., Berg, J. R., Jo, Y. H., Yeo, J. E., Nam, B. M., Koh, Y. G. and Lee, J. I. (2012). Trends in tissue engineering for blood vessels. *J. Biomed. Biotechnol.* **2012**, 956345.
Poché, R. A., Larina, I. V., Scott, M. L., Saik, J. E., West, J. L. and Dickinson, M. E. (2009). The Flk1-myr:mCherry mouse as a useful reporter to characterize multiple aspects of ocular blood vessel development and disease. *Dev. Dyn.* **238**, 2318-2326.
Polacheck, W. J., Charest, J. L. and Kamm, R. D. (2011). Interstitial flow influences direction of tumor cell migration through competing mechanisms. *Proc. Natl. Acad. Sci. USA* **108**, 11115-11120.
Roca, C. and Adams, R. H. (2007). Regulation of vascular morphogenesis by Notch signaling. *Genes Dev.* **21**, 2511-2524.
Sato, Y., Poynter, G., Huss, D., Filla, M. B., Czirok, A., Rongish, B. J., Little, C. D., Fraser, S. E. and Lansford, R. (2010). Dynamic analysis of vascular morphogenesis using transgenic quail embryos. *PLoS ONE* **5**, e12674.
Sengupta, A., Chakraborty, S., Paik, J., Yutzey, K. E. and Evans-Anderson, H. J. (2012). FoxO1 is required in endothelial but not myocardial cell lineages during cardiovascular development. *Dev. Dyn.* **241**, 803-813.
Sherman, T. F. (1981). On connecting large vessels to small. The meaning of Murray's law. *J. Gen. Physiol.* **78**, 431-453.
Song, J. W. and Munn, L. L. (2011). Fluid forces control endothelial sprouting. *Proc. Natl. Acad. Sci. USA* **108**, 15342-15347.
Szczerba, D., Kurz, H. and Szekely, G. (2009). A computational model of intussusceptive microvascular growth and remodeling. *J. Theor. Biol.* **261**, 570-583.
Taber, L. A., Ng, S., Quesnel, A. M., Whatman, J. and Carmen, C. J. (2001). Investigating Murray's law in the chick embryo. *J. Biomech.* **34**, 121-124.
Takahashi, T., Takahashi, K., St John, P. L., Fleming, P. A., Tomemori, T., Watanabe, T., Abrahamson, D. R., Drake, C. J., Shirasawa, T. and Daniel, T. O. (2003). A mutant receptor tyrosine phosphatase, CD148, causes defects in vascular development. *Mol. Cell. Biol.* **23**, 1817-1831.
Tardy, Y., Resnick, N., Nagel, T., Gimbrone, M. A., Jr and Dewey, C. F., Jr (1997). Shear stress gradients remodel endothelial monolayers in vitro via a cell proliferation-migration-loss cycle. *Arterioscler. Thromb. Vasc. Biol.* **17**, 3102-3106.
Thoma, R. (1893). *Untersuchungen über die Histogenese und Histomechanikdes Gefässsystems*. Stuttgart: Ferdinand Enke.
Tricot, O., Mallat, Z., Heymes, C., Belmin, J., Lesèche, G. and Tedgui, A. (2000). Relation between endothelial cell apoptosis and blood flow direction in human atherosclerotic plaques. *Circulation* **101**, 2450-2453.
Tzima, E., Irani-Tehrani, M., Kiosses, W. B., Dejana, E., Schultz, D. A., Engelhardt, B., Cao, G., DeLisser, H. and Schwartz, M. A. (2005). A mechanosensory complex that mediates the endothelial cell response to fluid shear stress. *Nature* **437**, 426-431.
Udan, R. S. and Dickinson, M. E. (2010). Imaging mouse embryonic development. *Methods Enzymol.* **476**, 329-349.
Udan, R. S., Culver, J. C. and Dickinson, M. E. (2013). Understanding vascular development. *Wiley Interdiscip. Rev. Dev. Biol.* **2**, 327-346.
Yuan, L., Sakamoto, N., Song, G. and Sato, M. (2012). Migration of human mesenchymal stem cells under low shear stress mediated by mitogen-activated protein kinase signaling. *Stem Cells Dev.* **21**, 2520-2530.
Zeng, G., Taylor, S. M., McColm, J. R., Kappas, N. C., Kearney, J. B., Williams, L. H., Hartnett, M. E. and Bautch, V. L. (2007). Orientation of endothelial cell division is regulated by VEGF signaling during blood vessel formation. *Blood* **109**, 1345-1352.
Zheng, Y., Chen, J., Craven, M., Choi, N. W., Totorica, S., Diaz-Santana, A., Kermani, P., Hempstead, B., Fischbach-Teschl, C., López, J. A. et al. (2012). In vitro microvessels for the study of angiogenesis and thrombosis. *Proc. Natl. Acad. Sci. USA* **109**, 9342-9347.